Control design of DC Microgrid Considering CPL Instability

Akhilesh Kumar Meena
Department of Electrical Engineering
Indian Institute of Technology (BHU)
Varanasi, India
akhileshkr.meena.eee21@itbhu.ac.in

Akrisht Vishwas
Department of Electrical Engineering
Indian Institute of Technology (BHU)
Varanasi, India
akrisht.vishwas.eee21@itbhu.ac.in

Dr. Avirup Maulik
Assistant Professor, Department of Electrical Engineering
Indian Institute of Technology (BHU)
avirupmaulik.eee@itbhu.ac.in

***Abstract*— This study explores the dynamics of a DC microgrid system integrating an uncontrollable solar unit and a controllable unit to supply a constant power load (CPL). Employing a buck converter architecture, we address CPL-induced instability by introducing a virtual conductance into the control scheme. Through the derivation of the state space equation and the assessment of participation factors for various state variables, we identify the output voltage as the most influential factor. To counteract instability, we propose integrating a control variable of virtual conductance, Gv, with the output voltage when utilizing it as feedback. Then LQR parameters are also derived to ensure the stability of desired performance criteria This holistic approach offers insights into bolstering the stability and efficacy of DC microgrid systems, facilitating their seamless incorporation of renewable energy sources and constant power loads.**

Keywords—DC microgrid, Robust control, Constant power load, LQR optimal control

I. INTRODUCTION

The Rise of Microgrids: Distributed energy resources, also known as on-site generation, are increasingly being implemented near consumption points. These resources can be either uncontrollable and reliant on renewable sources like solar and wind (dispatchable), or controllable units like fuel cells and microturbines (non-dispatchable). A low or medium voltage network comprised of distributed generation, energy storage, and controllable loads forms a microgrid.

AC vs. DC Microgrids: While AC microgrids are currently dominant, DC microgrids are gaining traction in data centers, remote electrification projects, and smart buildings due to their inherent advantages.

Reduced Conversion Stages: Unlike AC systems that require DC-AC conversion for each renewable energy source or stage, DC microgrids eliminate the need for multiple converters, simplifying the system.

Enhanced Controllability: DC microgrids offer simpler control due to the absence of frequency and phase balancing concerns. In contrast, AC systems necessitate both voltage and frequency regulation, alongside phase balancing in three-phase systems.

Reduced Losses: DC microgrids inherently eliminate losses associated with reactive current, such as the skin effect.

Challenges of DC Microgrids: However, DC microgrids come with their own set of drawbacks.

Power Protection: The natural zero crossings present in AC systems allow for easy current interruption at minimal stored energy. DC systems lack these zero crossings, necessitating more complex and expensive protection schemes. While research continues, the economic viability of DC microgrid protection systems remains a challenge.

Stability with Constant Power Loads: Constant power loads (CPLs) can introduce instability in DC microgrids. This instability, arising as a negative resistance during small-signal analysis, can be compensated for by introducing a virtual conductance (Gv) in parallel with the negative resistance to achieve overall system stability.

Our Approach: This project explores methods for stabilizing DC microgrids. We will delve into the negative resistance phenomenon caused by CPLs and examine how a virtual conductance can be employed for system stabilization. Additionally, we will investigate the application of Linear Quadratic Regulator (LQR) optimal control to achieve system stability through the derivation and implementation of LQR parameters.

II. DC MICROGRID

A. *Components of DC Microgrid*

This project focuses on a DC microgrid system comprised of the following key elements:

Renewable Energy Source: A solar photovoltaic (PV) unit serves as the non-dispatchable (uncontrollable) source of renewable energy.

Power Regulation: A DC-DC buck converter, positioned between the non-dispatchable unit and the DC bus, regulates the incoming power to match the DC bus voltage.

DC Bus: The DC bus serves as the central artery of the system, interconnecting all power-generating and consuming components.

Constant Power Load: A constant power load represents the continuous power demand within the microgrid.

Dispatchable Power Source: A dispatchable unit, in this case a fuel cell, provides a controllable source of power to supplement or compensate for fluctuations in renewable energy generation.

Dispatchable Unit Converter: Similar to the non-dispatchable unit, a DC-DC buck converter ensures that the dispatchable unit's output aligns with the DC bus voltage.

B. *Dispatchable Unit : Buck Converter Analysis*

Within this DC microgrid, we establish a fixed DC bus voltage (Vbus) of 48V. This voltage is maintained by the

dispatchable fuel cell unit, which operates at a higher voltage (Vi) of 100V. To seamlessly integrate the fuel cell into the system, a DC-DC buck converter acts as a voltage regulator. It steps down the fuel cell's output voltage to precisely match the Vbus level.

The control system for this buck converter prioritizes output voltage regulation. It continuously monitors and adjusts the converter's operation to ensure the voltage at the DC bus (Vo) remains stable at the desired 48V reference value

It's important to note that while this specific system utilizes a buck converter, other suitable converter topologies can be implemented depending on the application, without affecting the generality of our analysis.

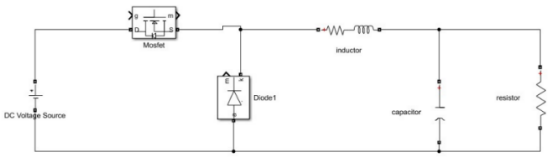

Fig. 1. Nominal Model of DC-DC Buck Converter

Our analysis of the buck converter will proceed in two stages:

Mode Breakdown: We will begin by dissecting the converter's operation into its two distinct states - "ON" and "OFF." This analysis will reveal how the circuit behaves when the switch is turned on and off.

State-Space Averaging: Following the mode breakdown, we will employ a technique known as state-space averaging. This technique allows us to simplify the complex, time-varying behavior of the converter into a more manageable average model.

When the switch is ON (Mode 1):

1)
$$V_i = L\frac{di}{dt} + i \cdot r_s + V_o$$

2)
$$i = C\frac{dV_o}{dt} + \frac{V}{R}$$

When the switch is OFF (Mode 2) :

1)
$$0 = L\frac{dV_o}{dt} + i \cdot r_s + V_o$$

2)
$$i = C\frac{dV_o}{dt} + \frac{dV_o}{dt}$$

These equations are obtained using Kirchhoff's Voltage and Current Laws.

Mode 1 operates for D · Ts where D represents the Duty Cycle of this Buck Converter and Ts represents the switching period i.e. the reciprocal of the switching frequency of the MOSFET used in the Buck Converter. Taking Ts = 10kHz as it is a standard value. Also Vi = 100V, Vo = 48V , thus the Duty Cycle will be D =Vi/Vo=0.48. Mode 2 whereas operates for time (1 − D) · Ts. Performing State Space Averaging by multiplying the above equations with the time for which they are applicable and finally adding the corresponding equations, we obtain :

1)
$$D \cdot v_i = L\frac{di}{dt} + ir_s + v_o$$

2)
$$i = C\frac{dv_o}{dt} + \frac{v_o}{R}$$

Now we want to Linearize this model under Steady State Conditions with a Small Ripple Approximation. Firstly, the Steady State Conditions means Do · Vi = Io · rs + Vo and Io=Vo/R. Then we will take the following approximations for linearization purposes:

$$D = D_o + d$$
$$v_o = V_o + \hat{v}$$
$$i = I_o + \hat{i}$$

Substituting these new approximations in the equations obtained by State Space Averaging and then simplifying further, we get the following equations :

1)
$$D_o\hat{v_i} + \hat{d}V_i = L\frac{d\hat{i}}{dt} + r_s\hat{i} + \hat{v}$$

2)
$$\hat{i} = C\frac{d\hat{v}}{dt} + \frac{\hat{v}}{R}$$

Now, Small-signal model is obtained by these equations.

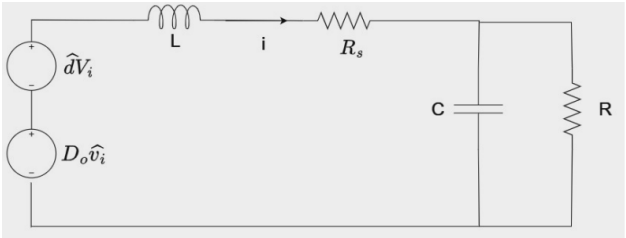

Fig. 2. Small Signal Average model of DC-DC Buck Converter

C. Integration with Solar PV cells

The Photovoltaic Unit and Power Extraction Optimization The DC microgrid incorporates a Solar Photovoltaic (PV) unit, a device comprised of numerous solar panels. This unit serves the crucial function of transforming solar energy into electrical energy with a direct current (DC) output. Since our microgrid operates on a DC platform, this eliminates the need for expensive DC-AC converters, a significant advantage. Instead, the PV unit's output can be directly connected to the DC bus link via an intermediate DC-DC buck converter for regulation.

MPPT for Optimal Power Extraction:
It's important to distinguish this buck converter from the one analyzed previously. In the prior case, the input voltage was fixed, and the control system focused on tracking and stabilizing the output voltage. Here, the scenario is reversed. The output voltage (Vo) of the DC bus link is already fixed

at 48V.Our objective becomes tracking the input voltage, which varies based on weather conditions. The generation capacity of the PV unit is directly influenced by ambient temperature and solar irradiation.

To extract the maximum possible power under these variable conditions, an algorithm known as Maximum Power Point Tracking (MPPT) is employed. This converter utilizes MPPT to dynamically adjust its operation and efficiently track the input voltage fluctuations. The goal is to maximize the power transferred from the PV unit to the DC bus link.

Figure 3 depicts the nominal model of this buck converter designed for MPPT operation.

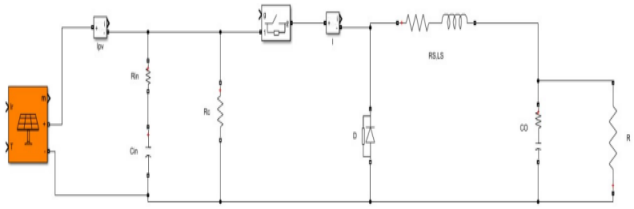

Fig. 3. Nominal Model of DC-DC Buck Converter connecting PV Unit to DC Bus Link

Once again, we will repeat the process done for the previous buck converter for this converter.

Equations for Mode 1 are:

1)

$$i_{pv} = C_i \frac{dV_i}{dt} + i + \frac{V_i}{R_c}$$

2)

$$V_i = L\frac{di}{dt} + R_s \cdot i + V_o$$

Equations for Mode 2 are:

1)

$$i_{pv} = C_i \frac{dV_i}{dt} + \frac{V_i}{R_c}$$

2)

$$0 = L\frac{di}{dt} + R_s \cdot i + V_o$$

Now we will do state space averaging. By taking Duty Cycle, D and Switching Frequency Ts. Mode 1 runs for D.Ts time and Mode 2 runs for (1 – D). Ts time. This will give following equations :

1)

$$i_{pv} = C_i \frac{dv_i}{dt} + D \cdot i + \frac{v_i}{R_c}$$

2)

$$D \cdot v_i = L\frac{di}{dt} + R_s \cdot i + v_o$$

Now we will linearize the above model under steady state conditions after taking appropriate approximations. That will yield the following small signal average model equations:

$$\hat{i_{pv}} = C_i \frac{d\hat{V_i}}{dt} + \hat{di}_o + D_o\hat{i}$$

$$D_o\hat{V_i} + \hat{d}V_{io} = L\frac{d\hat{i}}{dt} + R_s\hat{i}$$

III. Designing of Control System and Simulations on MATLAB

A. *Voltage Controller and Current Controller Design for Buck Converter*

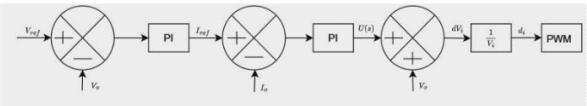

Fig. 4. Block Diagram of Control Loop in Dispatchable-side Converter

Our control system is designed to achieve optimal performance by utilizing voltage and current references. It leverages two Proportional-Integral (PI) controllers: a voltage controller and a current controller. These controllers analyze the difference between the reference values and the actual measurements (feedback) of voltage and current. Based on this error signal, the controllers generate corrective control actions. The output of these PI controllers ultimately provides feedback to the Pulse Width Modulation (PWM) generator. This PWM generator acts as the commander of the MOSFET switch, regulating its practical switching frequency. The impact of the control system on the MOSFET's switching behavior is depicted in Figure 4.We will Apply Laplace Transform on the equations that were derived in the previous Section, taking Vi as a constant input (it is provided by means of an ideal fuel cell).This will give equations:

1)

$$U(s) = s \cdot LI(s) + R_sI(s)$$

2)

$$I(s) = s \cdot CV(s) + \frac{V(s)}{R}$$

From the above equations , we get transfer functions of voltage and current controllers. We have to find values of PI constants for the PI controllers. The transfer functions of current and voltage controllers are respectively:

1)

$$\frac{I(s)}{U(s)} = \frac{1}{R_s + sL}$$

2)

$$\frac{V(s)}{I(s)} = \frac{R}{1 + sRC}$$

We will use the concept of Pole-Zero Cancellation in order to select the optimal values of Kp and Ki . Let us start with the analysis of the inner controller i.e. the current controller as seen in figure 4. Let G(s) denote the open-loop transfer function of the current controller and its plant cascaded together. i.e.

$$G(s) = \frac{sK_p + K_i}{s(R_s + sL)} = \frac{K_i(1 + \frac{sK_p}{K_i})}{sR_s(1 + \frac{sL}{R_s})}$$

For the purpose of smooth operation of the system, we take the bandwidth of this system to be 10 times that of the Switching Frequency of the PWM Generator.

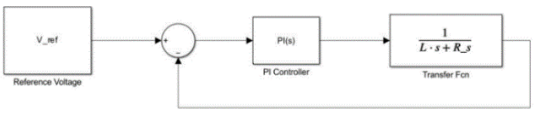

Fig. 4. Block Diagram of Current Controller and its corresponding Plant

For Pole-Zero Cancellation in G(s), we shall choose values of Kp and Ki such that

$$\frac{K_p}{K_i} = \frac{L}{R_s}$$

Therefore,

$$G(s) = \frac{K_i}{s \cdot R_s}$$

Closed loop transfer function will be,

$$G_{CL}(s) = \frac{K_i}{K_i + R_s \cdot s} = \frac{1}{1 + s \cdot (\frac{R_s}{K_i})}$$

We take this bandwidth to be 20 times the Switching Frequency, thus

$$\frac{1}{\tau} = \frac{2\pi f_s}{20}$$

Thus

$$\tau = \frac{R_s}{K_i} = \frac{20}{2\pi f_s}$$

Thus,

$$K_i = \frac{2\pi f_s R_s}{20}$$

Now from the relation $\frac{K_p}{K_i} = \frac{L}{R_s}$, we can also obtain that

$$K_p = \frac{2\pi f_s L}{20}$$

Thus we have get values of Kp and Ki for current controller. Now we will find Kp and Ki for voltage controller. The outer loop, functioning as the voltage controller, operates at a considerably slower pace (approximately 10 times slower) compared to the inner current controller loop. This not only sets the bandwidth of the voltage controller and its plant but also causes the closed-loop reduction of the current controller and its plant to behave akin to a unity gain block concerning the voltage controller. Consequently, this establishes a control loop as depicted in Figure 5. Once more, defining the open-loop transfer function G(s) entails cascading the PI controller and its plant's transfer function. Therefore,

$$G(s) = \frac{(sK_p + K_i)R}{s(1 + sCR)} = \frac{RK_i(1 + \frac{sK_p}{K_i})}{s(1 + sCR)}$$

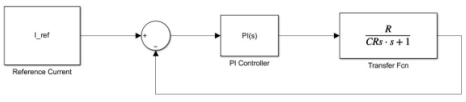

Fig. 5. Block Diagram of Voltage Controller and its corresponding Plant

According to Pole-Zero Cancellation in G(s), we will choose values of Kp and Ki such that,

$$\frac{K_p}{K_i} = RC$$

Therefore,

$$G(s) = \frac{R \cdot K_i}{s}$$

. Therefore, Closed-Loop Transfer Function

$$G_{CL}(s) = \frac{R \cdot K_i}{R \cdot K_i + s} = \frac{1}{1 + s \cdot (\frac{1}{R \cdot K_i})}$$

We will make this some ten times slower than the current controller. Then,

$$\frac{1}{\tau} = \frac{2\pi f_s}{200}$$

Thus

$$\tau = \frac{1}{R \cdot K_i} = \frac{200}{2\pi f_s}$$

Thus,

$$K_i = \frac{2\pi f_s}{200R}$$

Now from the relation $\frac{K_p}{K_i} = RC$, we can also obtain that

$$K_p = \frac{2\pi f_s C}{200}$$

Thus we have chosen values for K_p and K_i for the Voltage Controller as well.

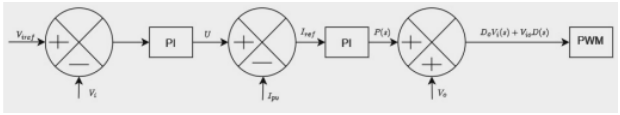

Fig. 6. Block Diagram of Control Loop of Non-Dispatchable Side Converter

B. *Controller Design for Buck Converter between PV Unit and DC Bus Link*

In our analysis of the Small Signal Average model concerning the buck converter linking the Solar PV Unit and the DC Bus, we previously derived the following equations:

$$\hat{i_{pv}} = C_i \frac{d\hat{V_i}}{dt} + \hat{di_o} + D_o\hat{i}$$

$$D_o\hat{V_i} + \hat{d}V_{io} = L\frac{d\hat{i}}{dt} + R_s\hat{i}$$

Taking the Laplace Transform of these equations, we get:

$$s \cdot C_iV_i = I_{pv} - I_oD - D_oI - \frac{V_i}{R_c}$$

$$s \cdot LI = D_oV_i + V_{io}D - R_sI - V_o$$

Which can further be simplified, if we consider $U(s) = I_{pv} - I_oD - D_oI$ and $M(s) = D_oV_i + V_{io}D - R_sI - V_o$ as:

$$\frac{V_i(s)}{U(s)} = \frac{R_c}{1 + sR_cC_i}$$

$$\frac{I(s)}{M(s)} = \frac{1}{R_s + sL}$$

Please note that the methodology employed here is identical in dimension to that conducted in the preceding subsection. It's also worth noting that throughout the entire Pole-Zero Cancellation Process, the input and output variables of the transfer function are of no concern; rather, we focus solely on the form of the transfer function. Therefore, we can assert that the same Pole-Zero Process applied to this buck converter will yield identical outcomes. In other words, the formulas for Kp and Ki for both the Current and Voltage Controllers will remain unchanged. Nonetheless, certain adjustments may occur, such as R being substituted with Rc in specific instances. Hence, we can conclude that for the Current Controller:

$$K_i = \frac{2\pi f_s R_s}{20}$$

$$K_p = \frac{2\pi f_s L}{20}$$

And for the Voltage Controller :

$$K_i = \frac{2\pi f_s}{200 R_c}$$

$$K_p = \frac{2\pi f_s C_i}{200}$$

C. *Preliminary Simulation of the Buck Converter Connecting the Dispatchable Unit to the DC Bus Link*

We will proceed to conduct a simulation of the fundamental buck converter model alongside its control system using MATLAB Simulink. Illustrated in Figure 7 is the circuit as simulated in MATLAB Simulink. Concurrently, Figure 8 presents the output waveforms of this converter. The first waveform depicts the PWM Generator, while the second waveform illustrates the current flowing through the inductor. Lastly, the third and final waveform portrays the output voltage, which is sustained across the DC Bus Link. It is evident that the output voltage remains stable at 48V, exhibiting approximately 2% ripple content.

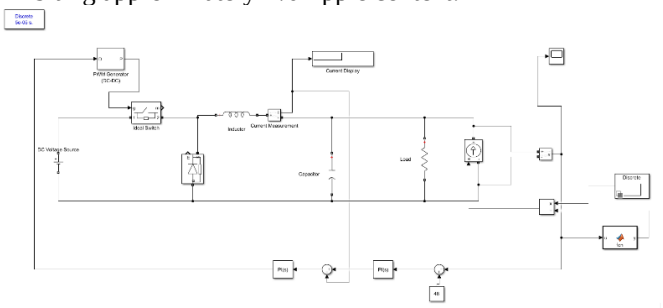

Fig. 7. MATLAB Simulink circuit of DC-DC Buck Converter between Dispatchable Unit and DC Bus Link with control system

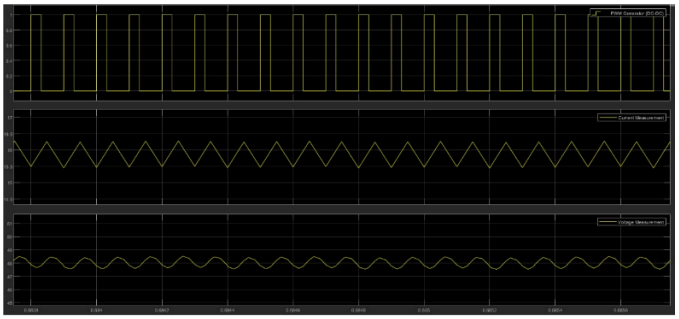

Fig. 8. Output waveforms of DC-DC Buck Converter between Dispatchable Unit and DC Bus Link with control system as seen in MATLAB Simulink

D. *Prelimnary Simulation of Buck Converter Connecting PV Unit to DC Bus Link*

We will proceed with a MATLAB Simulink simulation of the fundamental circuit for the DC-DC Buck Converter connecting the PV Unit to the DC Bus Link. It's worth noting our utilization of stair generators at different points to simulate fluctuating quantities, such as irradiation and load variations. Figure 9 displays the circuit as simulated in MATLAB Simulink, while Figure 10 illustrates the input voltage waveform, which is the focus of our tracking efforts in this specific converter.

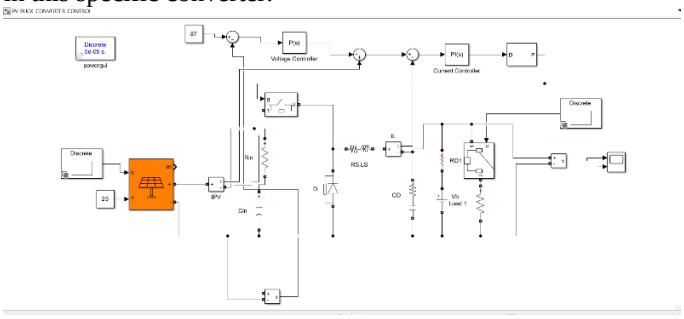

Fig. 9. MATLAB Simulink circuit of DC-DC Buck Converter between PV Unit and DC Bus Link with control system

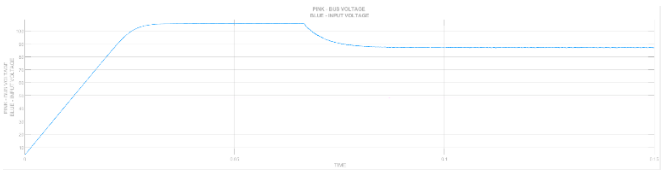

Fig. 10. PV-side Voltage waveform of DC-DC Buck Converter between PV Unit and DC Bus Link with control system as seen in MATLAB Simulink

IV. Instability due to Constant Power Load and Virtual Conductance

We will first address the challenge arising from the integration of Constant Power Loads (CPL) within our DC Microgrid system. To understand the instability originating from CPL, let's conduct a small signal analysis of a nominal network under steady-state conditions. Considering P0, V0, and I0 as the steady-state values of power, voltage, and current respectively, we can infer that :

$$P = VI$$

$$P_o + \Delta p = (V_o + \Delta v)(I_o + \Delta i)$$

$$\Delta p = \Delta v I_o + V_o \Delta i$$

$$\Delta i = \frac{\Delta p}{V_o} - \frac{\Delta v}{\left(\frac{V_o}{I_o}\right)}$$

$$\Delta i = \frac{\Delta p}{V_o} - \frac{\Delta v}{R_{cpl}}$$

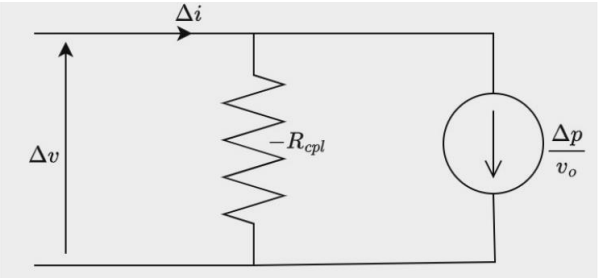

Fig. 11. Small Signal Model of Constant Power Load Nominal Network

Upon constructing the corresponding Small Signal Model, depicted in Figure 11, it becomes apparent that a term of negative resistance, denoted as -R_{cpl}, emerges within the model. This negative resistance serves as the primary instigator of instability within the physical framework of this network.

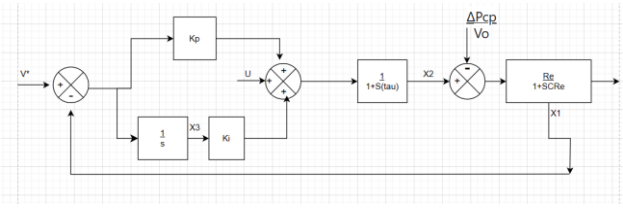

Fig. 12. Block Diagram of Combined Model of the DC Microgrid System

We will now analyze the block diagram (figure 17) of combined model of the DC Microgrid, to obtain a State Space Model. We get the State space model of this system as :

$$\begin{bmatrix} \dot{x}_1 \\ \dot{x}_2 \\ \dot{x}_3 \end{bmatrix} = \begin{bmatrix} \frac{-1}{R_e C} & \frac{1}{C} & 0 \\ \frac{-K_P}{\tau_1} & \frac{-1}{\tau_1} & \frac{K_I}{\tau_1} \\ -1 & 0 & 0 \end{bmatrix} \begin{bmatrix} x_1 \\ x_2 \\ x_3 \end{bmatrix} + \begin{bmatrix} \frac{-1}{CV_o} \\ \frac{K_p}{\tau_1} \\ V* \end{bmatrix} \begin{bmatrix} \Delta P_c p \\ V* \\ U \end{bmatrix}$$

We will now find the eigenvalues of this state matrix for the varying CPL :

Eigen Values				
R	-1	1	-2	2
λ1	4.5037+9.3398i	-5.345 + 9.773i	9.4294 + 3.292i	-1.0268 + 0.523i
λ2	4.5037-9.3398i	-5.345 - 9.773i	9.4294 - 3.292i	-1.0268 - 0.523i
λ3	-0.2385	-0.2065	-0.2570	-0.0193

We can see that for R= -1 ohms and R= -2 ohms , eigen values are on the right side of the plane which indicates instability of the system under negative resistance. In order to compensate for this instability, we will introduce a Virtual Conductance Gv in parallel with the CPL as seen in figure 13.

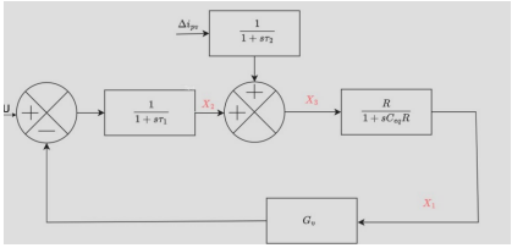

Fig. 13. Block Diagram with Gv implementation

Now we will find participation factor of state matrix to find which mode is most dominant.After finding participation factors of state matrix we can conclude that since State X1 i.e output voltage is the one which participates most in mode 1, which is the mode to be stabilized, hence we should give feedback from X1 i.e. Output Voltage. Hence Feedback of Gv is given from output voltage in figure 13

After the addition of Gv feedback, the new State Matrix becomes :

$$\begin{bmatrix} \frac{-1}{R_e C} & \frac{1}{C} & 0 \\ \frac{-G_v}{\tau} & \frac{-1}{\tau} & 0 \\ -1 & 0 & 0 \end{bmatrix}$$

Now checking the eigenvalues again for varying CPL yields the following :

Eigen Values				
R	-1	1	-2	2
λ1	-0.0109 + 1.2224i	-0.0205 + 1.226i	-0.0133 + 1.2225i	-0.0181 + 1.2225i
λ2	-0.0109 - 1.2224i	-0.0205 - 1.226i	-0.0133 - 1.2225i	-0.0181 - 1.2225i
λ3	-3.1416	-0.0314	-0.0314	-0.0314

Please note R is in Ohms in the table.

Here all modes lie in the left-half plane, which means that the system has been stabilized. In this way, we have solved the problem of Instability due to CPL with the help of Virtual Conductance.

V. Linear Quadratic Regulator (LQR) optimal control

We are further stabilising the output voltage which is the major influential factor by LQR optimal control.

Linear Quadratic Regulator (LQR) is a control algorithm used in the field of control systems engineering. It is designed to optimize the performance of linear dynamic systems by minimizing a quadratic cost function over an infinite time horizon. LQR aims to achieve a desired system performance while minimizing a cost function. This cost function typically balances two factors:

State deviations: We penalize how much the system's state variables (output voltage) deviate from their desired values.

Control effort: We also penalize the magnitude of the control input itself. A large control effort might be undesirable due to energy consumption or actuator limitations.

LQR is applicable to linear time-invariant systems described by state-space equations of the form:

$$\dot{x} = Ax + Bu$$

$$y = Cx$$

Where, x is the state vector representing the system's internal states, u is the control input vector, y is the output vector, A is the state matrix, B is the input matrix, C is the output matrix.

The performance criterion in LQR is typically defined as the sum of the weighted quadratic costs of the state and control input variables. The cost function is given by:

$$J = \int_0^\infty (x^T Q x + u^T R u) dt$$

where, Q is the state weighting matrix, R is the control input weighting matrix.

In LQR (Linear Quadratic Regulator) control, two key matrices play a significant role: the state weighting matrix (Q) and the control input weighting matrix (R). Here's an explanation of each:

1. State Weighting Matrix (Q):

The state weighting matrix, denoted as Q, represents the relative importance assigned to each state variable in the system. It is a symmetric positive semi-definite matrix of size (n times n), where (n) is the number of state variables in the system. The elements of Q determine how deviations from the desired state values contribute to the overall cost function.

2. Control Input Weighting Matrix (R):

The control input weighting matrix, denoted as R, represents the relative importance assigned to each control input variable in the system. It is a symmetric positive definite matrix of size (m times m), where (m) is the number of control input variables in the system. Similar to Q, the elements of R determine how control efforts contribute to the overall cost function.

the goal of LQR is to find the optimal control law u(t) that minimizes the cost function J over an infinite time horizon. This is achieved by solving the associated Riccati differential equation, known as the continuous-time algebraic Riccati equation (CARE), which provides the optimal state-feedback gain matrix K. Once the optimal gain matrix K is obtained, the control law u(t) is determined as:

$$u(t) = -Kx(t)$$

Where K is the optimal state-feedback gain matrix.

We will the state space model that is already created in previous section to implement the LQR optimal control.

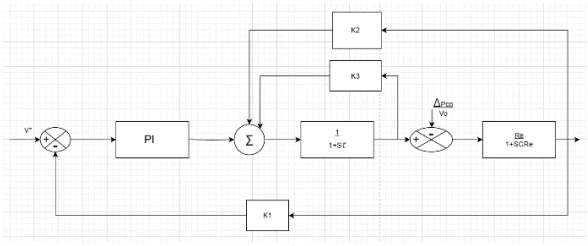

Fig. 14. Block Diagram of LQR implementation

We calculated values of K_1, K_2, K_3 using MATLAB function and proceed with MATLAB Simulink simulation of the fundamental circuit for the DC-DC Buck Converter connecting the PV Unit to the DC Bus Link with the LQR state- gain feedback. Figure 15 displays the circuit as simulated in MATLAB Simulink, while Figure 16 illustrates the output voltage waveform.

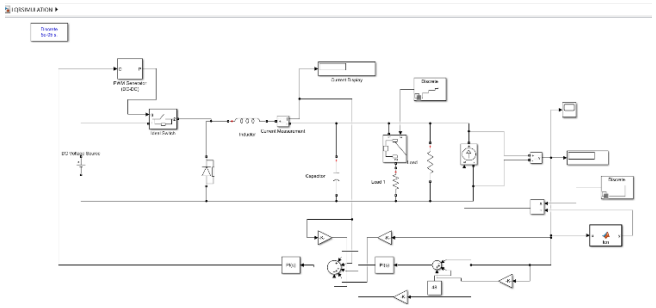

Fig. 15. MATLAB Simulink circuit of DC-DC Buck Converter between PV Unit and DC Bus Link with LQR optimal control

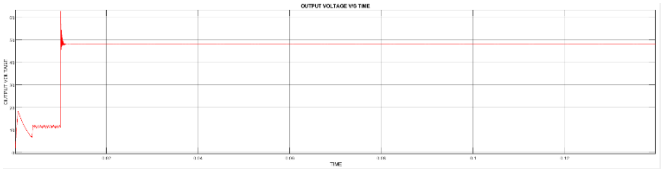

Fig. 16. Output voltage waveform with LQR optimal control.

VI. Conclusion

In this project we have shown in theory and with the help of simulations how we can combat the instability due to CPL with implementing Virtual Conductance and LQR state-gain feedback. respectively into the Control System Design of the DC Microgrid. We can see that with normal R load the output voltage was at 48.05 V , when we replace load with CPL , output voltage shows ripple from 47V to 49.1V, then we introduce virtual conductance to tackle this instability and ripple in output voltage reduces to from 47.2V to 48.2V. Now, to further stabilize the load we implemented LQR optimal control and output voltage becomes constant at 48.077V.

Acknowledgment

The authors would like to thank our mentor, Dr. Avirup Maulik for his guidance throughout the course of this project and for mentoring us with such enthusiasm and imparting us with very precious knowledge even beyond the scope of just this paper. Special thanks also to the Department of Electrical Engineering for providing us with the opportunity to work under such an experienced pool of professors and explore various aspects of Electrical Engineering through this B.Tech Project.

References

[1] R. H. Lasseter and P. Paigi, "Microgrid: a conceptual solution," 2004 IEEE 35th Annual Power Electronics Specialists Conference (IEEE Cat. No.04CH37551), Aachen, Germany, 2004, pp. 4285-4290 Vol.6, doi: 10.1109/PESC.2004.1354758. keywords: Distributed control;Power system reliability;Waste heat;Power

generation;Distribute power generation;Cogeneration;Engines;Mesh generation;Power system modeling;Inverters,

[2] F. S. Al-Ismail, ”DC Microgrid Planning, Operation, and Control: A Comprehensive Review,” in IEEE Access, vol. 9, pp. 36154- 36172, 2021, doi: 10.1109/ACCESS.2021.3062840. keywords: Microgrids;Planning;Reliability;Energy storage;Renewable energy sources;Supercapacitors;Batteries;DC microgrids;renewable energy sources;batteries;supercapacitors;dc bus voltage;power management;state of charge;microgrid operation;planning,

[3] Chen, Dong and Lie Xu. “Chapter 2 AC and DC Microgrid with Distributed Energy Resources.” (2019).

[4] R. M. Cuzner and G. Venkataramanan, ”The Status of DC Micro-Grid Protection,” 2008 IEEE Industry Applications Society Annual Meeting, Edmonton, AB, Canada, 2008, pp. 1-8, doi: 10.1109/08IAS.2008.382. keywords: Power system protection;Industrial power systems;Distributed control;Topology;Aircraft manufacture;Automotive engineering;Aerospace industry;Shipbuilding industry;Guidelines;Costs,

[5] E. Unamuno, J. Paniagua and J. A. Barrena, ”Unified Virtual Inertia for ac and dc Microgrids: And the Role of Interlinking Converters,” in IEEE Electrification Magazine, vol. 7, no. 4, pp. 56-68, Dec. 2019, doi: 10.1109/MELE.2019.2943978. keywords: Power system stability;Synchronous machines;Microgrids;DC machines;Perturbation methods;Power electronics